

Nuclear resonant scattering from ^{193}Ir as a probe of the electronic and magnetic properties of iridates

P. Alexeev,^{1,2} O. Leupold,¹ I. Sergueev,¹ M. Herlitschke,¹ D.F. McMorrow,³
R.S. Perry,³ E.C. Hunter,³ R. Röhlsberger,^{1,2,*} and H.-C. Wille^{1,†}

¹*Deutsches Elektronen-Synchrotron DESY, Notkestraße 85, 22607 Hamburg, Germany*

²*The Hamburg Centre for Ultrafast Imaging, Luruper Chaussee 149, 22761 Hamburg, Germany*

³*London Centre for Nanotechnology and Department of Physics and Astronomy,
University College London, Gower Street, London WC1E 6BT, United Kingdom*

(Dated: February 19, 2024)

The high brilliance of the modern synchrotron radiation sources facilitates experiments with high energy x-rays. In this Letter we report on Nuclear Resonance Scattering at the 73 keV nuclear level in ^{193}Ir . The transitions between the hyperfine split levels show an exceptionally large E2/M1 multipolarity mixing ratio combined with an increased sensitivity to certain changes in the hyperfine field direction compared to non-mixing transitions. The method opens a new way for probing local magnetic and electronic properties of correlated materials containing iridium and provides novel insights into their anisotropic magnetism. In particular, unexpected out-of-plane components of magnetic hyperfine fields and non-zero electric field gradients in Sr_2IrO_4 have been detected and attributed to the presence of strong spin-orbit interaction. Due to the high, 62 % natural abundance of the ^{193}Ir isotope, no isotopic enrichment of the samples is required, qualifying the method for a broad range of applications.

There is burgeoning interest in understanding the physical properties of systems which are simultaneously subject to strong spin-orbit coupling (SOC) and electron correlations, as exemplified by recent studies which have revealed a range of novel electronic and magnetic phases displayed by various 4d and 5d transition metal oxides (TMOs) [1–14].

At one level, SOC introduces another competing energy scale, producing unexpected electronic states. This is the case for the so-called spin-orbit Mott insulator in iridate perovskites which would otherwise be expected to be metallic in the absence of SOC. At another, more profound level, the SOC fully entangles spin and orbital degrees of freedom such that the magnetic interactions acquire an anisotropic, bond-directional nature – the Kitaev interaction – augmenting the conventional isotropic Heisenberg term which dominates 3d systems [9]. The resulting Kitaev-Heisenberg model is proving to be extremely rich displaying a plethora of topological quantum phases including spin-liquids, superconductivity, etc., the exploration of which is in its infancy [10, 15]. Further impetus for studying 4d and 5d TMOs stems from the rich possibilities offered by nano-structuring these materials, finding potential applications as biosensors, spintronic devices, catalysts, etc [16–19].

The iridate perovskites forming the Ruddlesden-Popper series of compounds $\text{Sr}_{n+1}\text{Ir}_n\text{O}_{3n+1}$ play a central role in the evolution of the field of systems combining SOC and electron correlations. Sr_2IrO_4 ($n=1$) was the first example of the new class of spin orbit Mott insulators which has attracted considerable interest due to the similarities of its magnetism, and to a certain extent its electronic structure, to La_2CuO_4 , the parent compound of high-temperature superconductors. Indeed potassium

doped onto the surface of Sr_2IrO_4 has been shown to induce a d-wave gap similar to that displayed by superconducting cuprates, although definitive proof of superconductivity in the iridate perovskites has not yet been produced. $\text{Sr}_2\text{I}_3\text{O}_7$ ($n=2$) is a marginal spin-orbit Mott insulator, in the sense that it can be transformed to unusual confined metallic phase (conducting in the ab plane only) for pressures above 55 GPa, although the details of key properties such as the magnetism of the high-pressure phase are unknown [3–5, 7, 13, 20, 21].

Indeed, revealing the nature of the electronic and magnetic correlations in iridates presents certain challenges which need to be overcome. These include the fact that the physics depends on a hierarchy of competing energy scales, requiring the characterisation of electronic and magnetic correlations over large ranges of energy and length scales. Second, single crystals of novel materials are often initially very small (in some cases no larger than 10 μm), meaning that methods with high sensitivity have to be developed. X-ray resonant scattering, both elastic (REXS) and inelastic (RIXS), from the Ir 4d electrons has proven to be especially useful, particularly so as neutron techniques are less suitable due to the low sensitivity of the technique and the high neutron absorption cross section of Ir.

In this Letter we establish synchrotron based nuclear resonance scattering (NRS) on ^{193}Ir at 73 keV as a complementary probe to REXS and RIXS for probing the electronic properties and magnetism of iridates. The main advantages of NRS are its exquisite sensitivity to the magnitude and direction of the electric and magnetic hyperfine fields, rendering it uniquely capable of revealing subtle changes to crystallographic and magnetic structures [22, 23]. Moreover, the high photon energy

of the ^{193}Ir resonance [24] opens the possibility of studying iridates under extreme conditions of pressure, such as the insulator to metal transition displayed by $\text{Sr}_3\text{Ir}_2\text{O}_7$ [8, 25].

Conventional Mössbauer spectroscopy on Ir has been performed several decades ago [24, 26], but did not become widespread, because the preparation of radioactive sources was notoriously difficult. NRS, on the other hand, does not require a radioactive source. Moreover, the narrow collimation and small beam size accessible at modern synchrotron radiation sources favor NRS studies of nanostructures [27, 28] and small samples at extremely high pressures and temperatures [22, 23, 29].

Natural Ir occurs in two stable isotopes, ^{191}Ir and ^{193}Ir . The 73 keV transition in ^{193}Ir with nuclear spins of $3/2$ and $1/2$ of ground and excited state, respectively, is most favorable for NRS studies due to the high, 62% natural abundance of the ^{193}Ir isotope and a comparatively long natural lifetime of 8 ns. The experiments were conducted at the Dynamics Beamline P01 at PETRA III (DESY, Hamburg) [30].

The storage ring was operated in 40-bunch top-up mode providing a stable 100 mA ring current. The experimental setup (Fig. 1(A)) included a double-crystal Si(311) monochromator which reduced the energy bandwidth of the 73 keV photons to about 8(1) eV. In order to reduce the energy bandwidth around the nuclear resonance in ^{193}Ir further, the energy bandwidth of photons transmitted by the sample was filtered via Bragg reflections from two specially designed Si crystals (F, Fig. 1(A)). The first crystal with an asymmetric (440) reflection collimates the beam for matching the acceptance of the subsequent (642) reflection which reduces the energy bandwidth to about 150 meV [31]. Tuning of the photon energy to that of the nuclear resonance and measurement of the lifetime of the excited state was performed by monitoring delayed nuclear fluorescence from an Ir metal foil by a large area avalanche photo diode (APD) detector (D_{inc} , Fig. 1(A)). The nuclear forward scattering (NFS) was detected by a fast detector array consisting of 16 APDs (D_{coh} , Fig. 1(A)) [31–33]. The fast detector array and very high bunch purity in the PETRA storage ring enabled the counting of delayed photons as early as 3 ns after the excitation pulse with a time resolution of about 0.6 ns [31].

The nuclear resonance was found 3.211 keV below the K-edge of Ir at 76.111 keV, and its energy was determined to 72.90(8) keV. This value is in good agreement with the frequently reported literature value of 73.0(5) keV [34], though it is lower than the more precise value 73.045(5) keV obtained in Ref. [35] from the measurement of internal conversion. The reason for the latter is unclear as in both measurements the maximum of the derivative of the edge absorption curve was used as a reference. Furthermore, the reference value of the edge

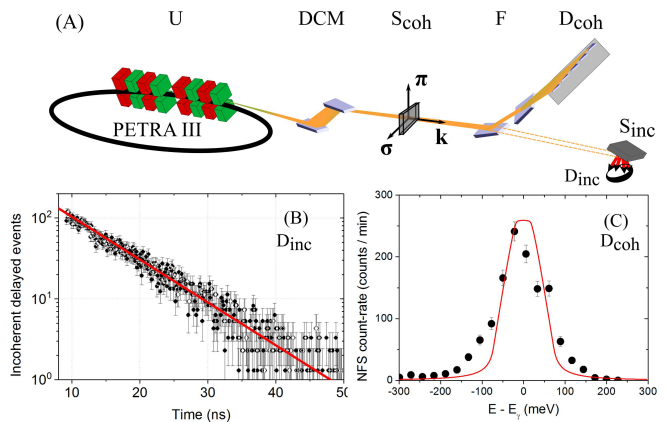


FIG. 1. (A): experimental setup with U - undulator source, DCM - double crystal monochromator, F - filtering optics, D_{coh} and D_{inc} - nuclear forward and nuclear fluorescence APD detector, respectively, and S_{coh} and S_{inc} - samples for forward and incoherent scattering experiment, respectively. (B): time spectrum of delayed nuclear fluorescence (black dots) and exponential decay with time constant $\tau_0 = 8.4(2)$ ns (red line). (C): spectrum of coherent delayed events. The red line shows the instrumental function predicted by the dynamical theory of x-ray diffraction.

used in [35] is 76.101 keV, which increases the disagreement. Fitting the time spectrum of delayed nuclear fluorescence with an exponential decay function (Fig. 1(B)), we determined the natural lifetime to be 8.4(2) ns, in accordance with the lifetime value of 8.8(2) ns reported in Ref. [34] and slightly lower than the one reported in [35] of 8.78 ns (no error given).

The corresponding resonance linewidth is 78(2) neV. Using the NFS setup, we measured an instrumental function of the filtering optics (Fig. 1(C)). Its width of 158(8) meV (FWHM) is close to that of 112 meV (FWHM) predicted by dynamical theory (Fig. 1(C), red line). The broadening can be related to the imperfections in the bulk silicon utilized for the crystals.

In order to demonstrate the feasibility of the technique we performed NFS measurements on elemental Ir and on IrO_2 . Both materials have been studied earlier by conventional Mössbauer spectroscopy [36]; these are used here as references for validation of data treatment routines in the time domain. While elemental Ir shows a single resonance line, Ir in IrO_2 exhibits an Ir^{4+} state with a pure electric hyperfine interaction [36]. NRS time spectra of 100 μm thick foil of elemental Ir have been acquired in half an hour (Fig. 2(A)) at signal count rates of about 7 s^{-1} . We observed a shift of beating minima to later times with increasing temperature due to the decrease of Lamb-Mössbauer factor (Fig. 2(A), lower graphs). Since the temporal beating pattern can be fully described as dynamical beats [37], hyperfine interactions can be ruled out, in accordance with the cubic lattice and paramagnetism of the elemental Ir [38]. Fitting the

temperature dependence of the Lamb-Mössbauer factor with the Debye model [39], we determined a Debye temperature of 309(30)K. This value is in good agreement with the literature value of 335(13) K [40].

NFS time spectra of the IrO_2 powder sample are shown in Fig. 2 (B). Fitting of the experimental data (Fig. 2 (B), upper graph) was performed with the CONUSS software [41]. To take the high mixing ratio of the E2/M1 multipole radiation into account [36, 42] CONUSS had to be extended. Special cases of the NRS theory for ferromagnetic and anti-ferromagnetic arrangements considering high mixing ratios are rolled out in detail in the Supplemental Material [31]. Where suitable, a comparison to the simple M1 case in ^{57}Fe is also given.

Fitting the data resulted in a quadrupole splitting $\Delta E_Q = \frac{eQV_{zz}}{2}$ of 2.76(2) mm/s ($8.96(7)\Gamma_0$) was obtained (e is the elementary charge, Q is the quadrupole moment, V_{zz} is the electric field gradient (EFG) along the quantization axis). This value is in excellent agreement with the value of 2.71(6) mm/s reported in Ref. [43]. We obtained an axially symmetric EFG with $V_{zz} = 1.71(1) \cdot 10^{18}$ V/cm² which is two orders of magnitude higher than in the isostructural 4d-RuO₂ reported in Ref. [44]. The EFG in IrO_2 is therefore mostly determined by valence 5d-electrons because of: (i) three times lower shielding of the Ir nucleus from the valence electrons than from the surrounding ions [36, 45] and (ii) more elongated 5d-orbitals in IrO_2 providing a potentially higher EFG [39]. In order to measure the isomer shift of Ir^{4+} in IrO_2 , we introduced an Ir metal foil as a single line reference absorber and acquired a NFS time spectrum of the combined setup (Fig. 2 (B), lower graph). From the evaluation of this dataset we obtained an isomer shift of -0.89(5) mm/s in IrO_2 relative to Ir metal, which is in good agreement with the value of -0.93(1) mm/s reported in Ref. [46].

To develop the method for studies of magnetic materials, we measured NFS from the ferromagnetic alloy $\text{Fe}_{0.98}\text{Ir}_{0.02}$ in an external magnetic field of 0.53(5) T. Dilute alloys of $\text{Fe}_{1-x}\text{Ir}_x$ ($x \leq 0.1$) show nearly pure magnetic hyperfine interactions [47, 48], and the hyperfine fields in these alloys are the highest for all known compounds with d-elements [49]. The large hyperfine fields lead to very fast oscillations in the temporal beat patterns of NFS and therefore provide the best benchmark of time resolution of the setup. The NFS time spectrum of a 1.6 mm thick sample of $\text{Fe}_{0.98}\text{Ir}_{0.02}$ exhibits extremely fast oscillations with a period of ≈ 1.5 ns (Fig. 2 (C)).

Notably, despite the aforementioned high E2/M1 mixing ratio the $\text{Fe}_{0.98}\text{Ir}_{0.02}$ NFS spectrum shows a very regular beating pattern, significant for an (almost pure) two transition line spectrum. At a first glance this is surprising as even the pure M1 case (e.g. for ^{57}Fe) shows a more complicated spectrum. The reason for this is that due to the E2/M1 mixing parameter, which value is close the square root of 1/3, M1 and E2 transition amplitudes in the mixed M1/E2 case can cancel each other for specific

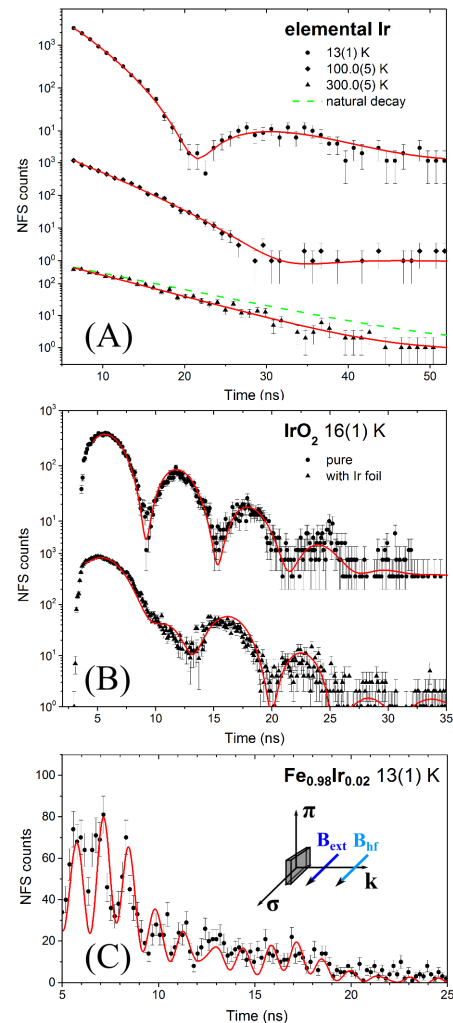


FIG. 2. NFS time spectra of: (A) Ir foil, (B) IrO_2 powder, (C) $\text{Fe}_{0.98}\text{Ir}_{0.02}$. Black markers show experimental data and the red lines show fits by nuclear dynamical scattering theory. Green dotted line in the lower graph of (A) shows the natural decay of the 73 keV state. For better visibility (C) is plotted in linear scale; the inset shows the scattering geometry, directions of external magnetic field B_{ext} and hyperfine field B_{hf} .

transitions in ^{193}Ir (for more details see Supplemental Material [31], part C). We refine the value of the hyperfine field to 133(1) T, which is in good agreement with the value of 140(2) T reported for $\text{Fe}_{0.973}\text{Ir}_{0.027}$ in Ref. [24].

Having validated the NRS technique by studying relevant reference samples, we applied it for exploring magnetism and electronic properties of two iridates from the series of $\text{Sr}_{n+1}\text{Ir}_n\text{O}_{3n+1}$ Ruddlesden-Popper phases, i.e. SrIrO_3 and Sr_2IrO_4 .

SrIrO_3 is a paramagnetic metal with electronic structure determined by both strong spin-orbit interaction and large electronic correlation at temperatures higher than 50 K [7, 50]. Due to its impact on the elec-

tronic anisotropy and EFG resulting from it, the spin-orbit interaction in SrIrO_3 can be studied by probing the quadrupole splitting of the ^{193}Ir nuclear levels [51]. For a SrIrO_3 powder sample we obtained a quadrupole splitting of $1.24(5)$ mm/s ($4.0(2)\Gamma_0$) at 15 K (Fig. 3 (A), upper graph), in very good agreement with the value of 1.26 mm/s measured at 4 K in Ref. [46]. Magnetic hyperfine interactions can be ruled out, in accordance with paramagnetism in this compound in the temperature range under scope [50]. The quadrupole splitting decreases with temperature and reaches a value of $1.08(5)$ mm/s ($3.5(2)\Gamma_0$) at 108 K (Fig. 3 (A), lower graph), which can be related to the presence of a gap in the electronic ground state. To the best of our knowledge, no change of Ir coordination symmetry is reported for the temperature range investigated. Therefore the temperature dependent change in quadrupole splitting can be exclusively addressed to the thermal population of electronic levels, supporting the evidence of semimetal-like electronic band structure [52] in SrIrO_3 and showing the decisive impact of the large distortions in IrO_6 octahedra onto the electronic structure in this compound.

It is the unique strength of the NRS technique to provide local information on the magnitude and orientation of magnetic fields and electric field gradients at the Ir sites [31]. This allowed us to gain new insights into the magnetic order of the Sr_2IrO_4 perovskite. Sr_2IrO_4 crystals have a form of platelets with lateral size of 2×3 mm² and thickness of about 30 - 70 μm ; the whole incident beam was accepted by the sample. The Sr_2IrO_4 sample was aligned with the (001) plane perpendicular to the incident beam (inset Fig. 3 (B,C)) and five crystals have been stacked in the same orientation along the beam in order to increase the NFS signal [31]. EDX and magnetisation measurements suggest slight oxygen deficiency in the Sr_2IrO_4 sample [31].

The temporal beat pattern in the time spectrum of Sr_2IrO_4 is determined by both magnetic and electric hyperfine interactions (Fig. 3 (B,C)). We obtained a hyperfine field of $24.2(2)$ T which is in a very good agreement with the value of 24 T reported by Mössbauer spectroscopy in Ref. [36]. Whilst NRS at ^{193}Ir shows high sensitivity to the orientation of hyperfine fields [31], the model with in-plane hyperfine fields fails to explain the measured time spectrum (Fig. 3 (B)). Taking into account oxygen deficiency [31] and associated distortion of tetragonal symmetry [53], the local symmetry of Ir in Sr_2IrO_4 permits the existence of magnetic components along the c-axis [3, 53]. Introducing a 30° tilting angle of hyperfine fields to the a-b plane into the model fit provides a very good statistical quality of the fit to the measured time spectrum (Fig. 3 (C)), supporting the existence of out-of-plane components of the magnetic field at the Ir sites which was not observed before. One has to note that the direction of hyperfine field and magnetic moment do not need to coincide [54]. Especially, the ef-

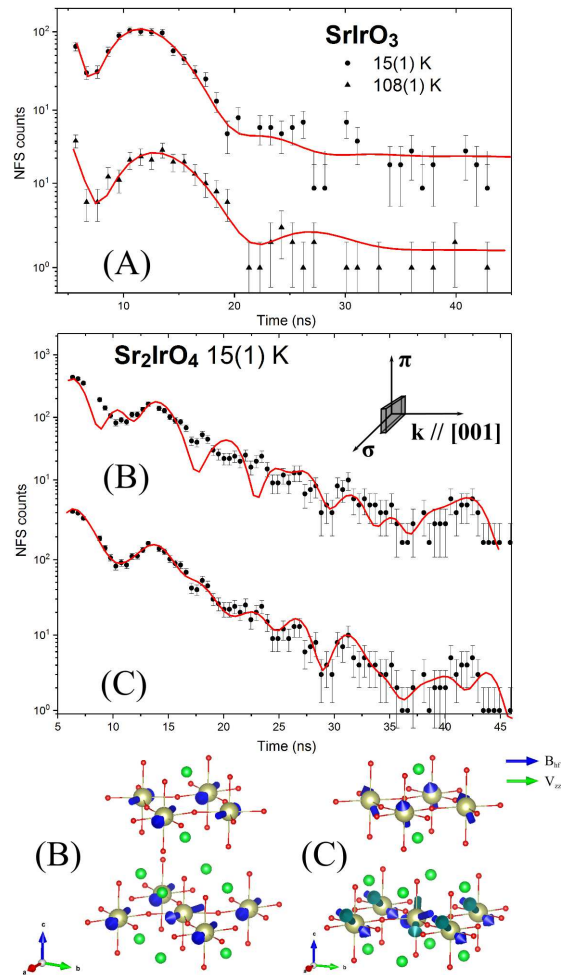


FIG. 3. (A): temperature dependent NFS time spectra of SrIrO_3 ; (B): NFS time spectra of Sr_2IrO_4 . The inset shows the scattering geometry. The red lines are fits by nuclear dynamical scattering theory: (B) assuming hyperfine fields in the basal plane and (C) with hyperfine planes tilted from the basal plane. The directions of the magnetic hyperfine fields B_{hf} and EFG quantization axes V_{zz} for the corresponding model fit in (B) and (C) are shown at the bottom .

fect is expected in the presence of significant orbital field contribution and interaction with the lattice as reported in Ref. [55]. An enhanced electronegativity of Ir also favors high covalency of Ir-O bonds, reducing the Fermi contact field and increasing the orbital field contribution to the hyperfine field [56–58]. In accordance with this statement, a strong anisotropy in electronic g -factors in Sr_2IrO_4 was observed by ESR in Ref. [59]. Considering the electric field at the Ir nuclei in Sr_2IrO_4 , we observe an axially symmetric EFG with a magnitude of $1.1(1) \cdot 10^{18}$ V/cm² in the [001] direction. The presence of an EFG is reasonable in view of distortion of the IrO_6 octahedra [3], oxygen deficiency, and the evidence of a non-zero EFG in the isostructural Sr_2RuO_4 [60]. The non-zero EFG in Sr_2IrO_4 and the out-of-plane

components of the magnetic hyperfine field found here might be addressed to the non-zero angular momentum of the outer electrons, arising from the reduced symmetry of the IrO_6 octahedra; temperature dependent measurements can provide further information on the origin of this phenomenon.

In conclusion, we have established Nuclear Resonance Scattering at the 72.90(8) keV level in ^{193}Ir as a new synchrotron-based technique for the studies of magnetism and electronic properties of iridates. A huge 133(1) T hyperfine field in dilute $\text{Fe}_{0.98}\text{Ir}_{0.02}$ alloy has been detected via NRS. Moreover, we found a thermally induced decrease of the electric field gradient across the Ir nuclei in SrIrO_3 and observed a non-zero EFG and tilting of hyperfine fields from the basal plane in Sr_2IrO_4 that should stimulate further investigations to relate structural and electronic properties in the iridates. All samples contained ^{193}Ir in its natural abundance; no preparation of radioactive sources is required and no line broadening due to the source is present. NRS at ^{193}Ir is sensitive to dilute systems and spin structures, providing a valuable input for studies to relate magnetism and spin-orbit interactions in iridates, e.g. in strong magnetic fields [4, 26], or under confinement in nanomaterials [16, 18, 19] and heterostructures [61]. The oxidation state of iridium and crystal fields at Ir ions can be tracked via measurements of isomer shift and quadrupole interactions at the Ir nucleus, respectively.

We acknowledge support of the Helmholtz association via project oriented funds. The PETRA machine operation group is gratefully acknowledged for establishing a beam cleaning procedure and maintaining high bunch purity. Wolfgang Sturhahn is greatly acknowledged for extending the CONUSS software for calculations of mixed multipole radiation. The authors are thankful to Hlynur Gretarsson, Christian Donnerer, and Raphaël P. Hermann for fruitful discussions on the physics of iridates. We thank Manfred Spiwek and Frank-Uwe Dill for the preparation of the silicon crystals and setup at the beamline. Thomas F. Keller (DESY NanoLab) is acknowledged for EDX measurements on Sr_2IrO_4 . Work at UCL was supported by the Engineering and Physical Sciences Research Council (grants EP/N027671/1 and EP/N034694/1).

* ralf.roehlsberger@desy.de

† hans.christian.wille@desy.de

- [1] Y. K. Kim, O. Krupin, J. D. Denlinger, A. Bostwick, E. Rotenberg, Q. Zhao, J. F. Mitchell, J. W. Allen, and B. J. Kim, “Fermi arcs in a doped pseudospin-1/2 Heisenberg antiferromagnet,” *Science* **345**, 187–190 (2014).
- [2] J. He, H. Hafiz, Th. R. Mion, T. Hogan, C. Dhital, X. Chen, Q. Lin, M. Hashimoto, D. H. Lu, Y. Zhang, R. S. Markiewicz, A. Bansil, S. D. Wilson, and Rui-Hua He, “Fermi Arcs vs. Fermi Pockets in Electron-doped Perovskite Iridates,” *Sci. Rep.* **5**, 8533 (2015).
- [3] M. K. Crawford, M. A. Subramanian, R. L. Harlow, J. A. Fernandez-Baca, Z. R. Wang, and D. C. Johnston, “Structural and magnetic studies of Sr_2IrO_4 ,” *Phys. Rev. B* **49**, 9198–9201 (1994).
- [4] B. J. Kim, H. Ohsumi, T. Komesu, S. Sakai, T. Morita, H. Takagi, and T. Arima, “Phase-sensitive observation of a spin-orbital mott state in Sr_2IrO_4 ,” *Science* **323**, 1329–1332 (2009).
- [5] S. Boseggia, H.C. Walker, J. Vale, R. Springell, Z. Feng, R.S. Perry, M.M. Sala, H.M. Rønnow, S.P. Collins, and D.F. McMorrow, “Locking of iridium magnetic moments to the correlated rotation of oxygen octahedra in Sr_2IrO_4 revealed by x-ray resonant scattering,” *J. Phys. Condens. Matter* **25**, 422202 (2013).
- [6] B. J. Kim, Hosub Jin, S. J. Moon, J.-Y. Kim, B.-G. Park, C. S. Leem, Jaejun Yu, T. W. Noh, C. Kim, S.-J. Oh, J.-H. Park, V. Durairaj, G. Cao, and E. Rotenberg, “Novel $J_{eff} = 1/2$ Mott State Induced by Relativistic Spin-Orbit Coupling in Sr_2IrO_4 ,” *Phys. Rev. Lett.* **101**, 076402 (2008).
- [7] S. J. Moon, H. Jin, K. W. Kim, W. S. Choi, Y. S. Lee, J. Yu, G. Cao, A. Sumi, H. Funakubo, C. Bernhard, and T. W. Noh, “Dimensionality-Controlled Insulator-Metal Transition and Correlated Metallic State in $5d$ Transition Metal Oxides $\text{Sr}_{n+1}\text{Ir}_n\text{O}_{3n+1}$ ($n = 1, 2, \text{ and } \infty$),” *Phys. Rev. Lett.* **101**, 226402 (2008).
- [8] C. Donnerer, Z. Feng, J. G. Vale, S. N. Andreev, I. V. Solovyev, E. C. Hunter, M. Hanfland, R. S. Perry, H. M. Rønnow, M. I. McMahon, V. V. Mazurenko, and D. F. McMorrow, “Pressure dependence of the structure and electronic properties of $\text{Sr}_3\text{Ir}_2\text{O}_7$,” *Phys. Rev. B* **93**, 174118 (2016).
- [9] G. Jackeli and G. Khaliullin, “Mott insulators in the strong spin-orbit coupling limit: From Heisenberg to a quantum compass and Kitaev models,” *Phys. Rev. Lett.* **102**, 017205 (2009).
- [10] W. Witczak-Krempa, G. Chen, Y.B. Kim, and L. Balents, “Correlated Quantum Phenomena in the Strong Spin-Orbit Regime,” *Annu. Rev. Condens. Matter Phys.* **5**, 57–82 (2014).
- [11] L. F. Mattheiss, “Electronic structure of RuO_2 , OsO_2 , and IrO_2 ,” *Phys. Rev. B* **13**, 2433–2450 (1976).
- [12] J. Kim, D. Casa, M. H. Upton, T. Gog, Y.-J. Kim, J. F. Mitchell, M. van Veenendaal, M. Daghofer, J. van den Brink, G. Khaliullin, and B. J. Kim, “Magnetic Excitation Spectra of Sr_2IrO_4 Probed by Resonant Inelastic X-Ray Scattering: Establishing Links to Cuprate Superconductors,” *Phys. Rev. Lett.* **108**, 177003 (2012).
- [13] Y. K. Kim, N. H. Sung, J. D. Denlinger, and B. J. Kim, “Observation of a d-wave gap in electron-doped Sr_2IrO_4 ,” *Nature Phys.* **12**, 37–41 (2016).
- [14] A. de la Torre, S. McKeown Walker, F. Y. Bruno, S. Riccò, Z. Wang, I. Gutierrez Lezama, G. Scheerer, G. Girit, D. Jaccard, C. Berthod, T. K. Kim, M. Hoesch, E. C. Hunter, R. S. Perry, A. Tamai, and F. Baumberger, “Collapse of the mott gap and emergence of a nodal liquid in lightly doped Sr_2IrO_4 ,” *Phys. Rev. Lett.* **115**, 176402 (2015).
- [15] R. Schaffer, E. Kin-Ho Lee, B.-J. Yang, and Y. B. Kim, “Recent progress on correlated electron systems with strong spinorbit coupling,” *Reports on Progress in Physics* **79**, 094504 (2016).

- [16] Z. C. Lin, C. Xie, Y. Osakada, Y. Cui, and B. Cui, “Iridium oxide nanotube electrodes for sensitive and prolonged intracellular measurement of action potentials,” *Nat. Commun.* **5**, 3206 (2014).
- [17] Zh. Qiu, D. Hou, T. Kikkawa, K. Uchida, and E. Saitoh, “All-oxide spin Seebeck effects,” *Appl. Phys. Express* **8**, 083001 (2015).
- [18] J. E. Hirsch, “Spin hall effect,” *Phys. Rev. Lett.* **83**, 1834–1837 (1999).
- [19] K. Fujiwara, Y. Fukuma, H. Matsuno, J. and Idzuchi, Y. Niimi, Y. Otani, and H. Takagi, “5d iridium oxide as a material for spin-current detection,” *Nat. Comm.* **4**, 2893 (2013).
- [20] Y. J. Yan, M. Q. Ren, H. C. Xu, B. P. Xie, R. Tao, H. Y. Choi, N. Lee, Y. J. Choi, T. Zhang, and D. L. Feng, “Electron-doped Sr_2IrO_4 : An analogue of hole-doped cuprate superconductors demonstrated by scanning tunneling microscopy,” *Phys. Rev. X* **5**, 041018 (2015).
- [21] F. Wang and T. Senthil, “Twisted Hubbard Model for Sr_2IrO_4 : Magnetism and Possible High Temperature Superconductivity,” *Phys. Rev. Lett.* **106**, 136402 (2011).
- [22] R. Röhlsberger, *Nuclear condensed matter physics with synchrotron radiation: basic principles, methodology and applications*, Springer Tracts in Modern Physics, Vol. 208 (Springer, Heidelberg, 2004).
- [23] E. Gerdau and H. DeWaard, eds., *Nuclear resonant scattering of synchrotron radiation*, Vol. 123-124 (Springer International Publishing, 1999).
- [24] F. Wagner and U. Zahn, “Mössbauer isomer shifts, hyperfine interactions, and magnetic hyperfine anomalies in compounds of iridium,” *Z. Phys.* **233**, 1–20 (1970).
- [25] Yang Ding, Liuxiang Yang, Cheng-Chien Chen, Heung-Sik Kim, Myung Joon Han, Wei Luo, Zhenxing Feng, Mary Upton, Diego Casa, Jungho Kim, Thomas Gog, Zhidan Zeng, Gang Cao, Ho-kwang Mao, and Michel van Veenendaal, “Pressure-induced confined metal from the mott insulator $\text{sr}_3\text{ir}_2\text{o}_7$,” *Phys. Rev. Lett.* **116**, 216402 (2016).
- [26] G. J. Perlow, W. Henning, D. Olson, and G. L. Goodman, “Hyperfine anomaly in ^{193}Ir by Mössbauer effect, and its application to determination of the orbital part of hyperfine fields,” *Phys. Rev. Lett.* **23**, 680–682 (1969).
- [27] R. Röhlsberger, J. Bansmann, V. Senz, K. L. Jonas, A. Bettac, O. Leupold, R. Ruffer, E. Burkel, and K. H. Meiwes-Broer, “Perpendicular Spin Orientation in Ultrasmall Fe Islands on W(110),” *Phys. Rev. Lett.* **86**, 5597–5600 (2001).
- [28] S. Stankov, R. Röhlsberger, T. Slezak, M. Sladeczek, B. Sepiol, G. Vogl, A. I. Chumakov, R. Ruffer, N. Spiridis, J. Lazewski, K. Parlinski, and J. Korecki, “Phonons in Iron: From the Bulk to an Epitaxial Monolayer,” *Phys. Rev. Lett.* **99**, 185501 (2007).
- [29] V. Potapkin, C. McCammon, K. Glazyrin, A. Kantor, I. Kuppenko, C. Prescher, R. Sinmyo, G.V. Smirnov, A.I. Chumakov, and R. Ruffer, “Effect of iron oxidation state on the electrical conductivity of the Earth’s lower mantle,” *Nat. Commun.* **4**, 1427 (2013).
- [30] Dynamics Beamline P01 web site, <http://photon-science.desy.de/facilities>.
- [31] See Supplemental Material at (URL will be inserted by publisher) for details on x-ray filter, APD detector array, beam cleaning in the PETRA ring, sensitivity of NRS to direction of hyperfine fields in iridates, and on alignment of the Sr_2IrO_4 single crystals which includes Refs. [22, 23, 33, 41, 42, 55, 62–65].
- [32] Alfred Q. R. Baron, Shunji Kishimoto, John Morse, and Jean-Marie Rigal, “Silicon avalanche photodiodes for direct detection of X-rays,” *Journal of Synchrotron Radiation* **13**, 131–142 (2006).
- [33] I. Sergueev, A. I. Chumakov, T. H. Deschaux Beaume-Dang, R. Ruffer, C. Strohm, and U. van Bürck, “Nuclear forward scattering for high energy Mössbauer transitions,” *Phys. Rev. Lett.* **99**, 097601 (2007).
- [34] E. Achterberg, O.A. Capurro, G.V. Marti, V.R. Vanin, and R.M. Castro, “Nuclear Data Sheets for $A = 193$,” *Nuclear Data Sheets* **107**, 1–224 (2006).
- [35] S. Kishimoto, Y. Yoda, Y. Kobayashi, S. Kitao, R. Haruki, and M. Seto, “Evidence for nuclear excitation by electron transition on ^{193}Ir and its probability,” *Nucl. Phys. A* **748**, 3–11 (2005).
- [36] F. E. Wagner, “Mössbauer spectroscopy with $^{191,193}\text{Ir}$,” *Hyperfine Interact.* **13**, 149–173 (1983).
- [37] J.P. Hannon and G.T. Trammell, “Coherent γ -ray optics,” *Hyperfine Interact.* **123**, 127–274 (1999).
- [38] H.J. Kandiner, *Iridium*, Gmelin Handbook of Inorganic and Organometallic Chemistry - 8th edition (Springer Berlin Heidelberg, 2013).
- [39] Ph. Gülich, E. Bill, and A. X. Trautwein, *Mössbauer Spectroscopy and Transition Metal Chemistry Fundamentals and Applications* (Springer, Heidelberg, 2011).
- [40] P. Steiner, E. Gerdau, W. Hautsch, and D. Steenzen, “Determination of the mean life of some excited nuclear states by Mössbauer experiments,” *Z. Phys. A* **221**, 281–290 (1969).
- [41] W. Sturhahn, “CONUSS and PHOENIX: Evaluation of nuclear resonant scattering data,” *Hyperfine Interact.* **125**, 149–172 (2000).
- [42] W. Sturhahn and E. Gerdau, “Evaluation of time-differential measurements of nuclear-resonance scattering of x-rays,” *Phys. Rev. B* **49**, 9285–9294 (1994).
- [43] U. Atzmony, E. R. Bauminger, D. Lebenbaum, A. Mustachi, S. Ofer, and J. H. Wernick, “Mössbauer effect in ^{193}Ir in intermetallic compounds and salts of iridium,” *Phys. Rev.* **163**, 314–323 (1967).
- [44] D. Bessas, D. G. Merkel, A. I. Chumakov, R. Ruffer, R. P. Hermann, I. Sergueev, A. Mahmoud, B. Klobes, M. A. McGuire, M. T. Sougrati, and L. Stievano, “Nuclear forward scattering of synchrotron radiation by ^{99}Ru ,” *Phys. Rev. Lett.* **113**, 147601 (2014).
- [45] P. Raghavan, E. N. Kaufmann, R. S. Raghavan, E. J. Ansaldo, and R. A. Naumann, “Sign and magnitude of the quadrupole interaction of ^{111}Cd in noncubic metals: Universal correlation of ionic and electronic field gradients,” *Phys. Rev. B* **13**, 2835–2847 (1976).
- [46] G. K. Shenoy and F.E. Wagner, “Mössbauer-Effect Isomer Shifts,” in *Mössbauer Spectroscopy Applied to Inorganic Chemistry*, edited by G. J. Long (Springer US, Boston, MA, 1984) pp. 57–76.
- [47] R.L. Mössbauer, M. Lengsfeld, W. von Lieres, W. Potzel, P. Teschner, F.E. Wagner, and G. Kaindl, “Nuclear gamma resonance study of the Ir–Fe and Ir–Ni alloy systems,” *Z. Naturforsch. A* **26**, 343 (1971).
- [48] D. Salomon and D. A. Shirley, “Quadrupole coupling at ^{193}Ir nuclei in iron,” *Phys. Rev. B* **9**, 29–31 (1974).
- [49] G.N. Rao, “Dilute-impurity hyperfine fields in Fe, Co, Ni, and Gd,” *At. Data Nucl. Data Tables* **15**, 553 – 576 (1975).

- [50] J.G. Zhao, L.X. Yang, Y. Yu, F.Y. Li, R.C. Yu, Z. Fang, L.C. Chen, and C.Q. Jin, “High-pressure synthesis of orthorhombic SrIrO_3 perovskite and its positive magnetoresistance,” *J. of Appl. Phys.* **103**, 103706 (2008).
- [51] R. Ingalls, “Electric-Field Gradient Tensor in Ferrous Compounds,” *Phys. Rev.* **133**, A787–A795 (1964).
- [52] Y. F. Nie, P. D. C. King, C. H. Kim, M. Uchida, H. I. Wei, B. D. Faeth, J. P. Ruf, J. P. C. Ruff, L. Xie, X. Pan, C. J. Fennie, D. G. Schlom, and K. M. Shen, “Interplay of Spin-Orbit Interactions, Dimensionality, and Octahedral Rotations in Semimetallic SrIrO_3 ,” *Phys. Rev. Lett.* **114**, 016401 (2015).
- [53] Feng Ye, S. Chi, B. C. Chakoumakos, J. A. Fernandez-Baca, T. Qi, and G. Cao, “Magnetic and crystal structures of Sr_2IrO_4 : A neutron diffraction study,” *Phys. Rev. B* **87**, 140406 (2013).
- [54] V. Schünemann and H. Winkler, “Structure and dynamics of biomolecules studied by Mössbauer spectroscopy,” *Rep. Prog. Phys.* **63**, 263 (2000).
- [55] H. Gretarsson, N. H. Sung, M. Höppner, B. J. Kim, B. Keimer, and M. Le Tacon, “Two-magnon raman scattering and pseudospin-lattice interactions in Sr_2IrO_4 and $\text{Sr}_3\text{Ir}_2\text{O}_7$,” *Phys. Rev. Lett.* **116**, 136401 (2016).
- [56] W. T. Oosterhuis and G. Lang, “Mössbauer effect in K_3FeCN_6 ,” *Phys. Rev.* **178**, 439–456 (1969).
- [57] J.C.M. Henning, “Covalency and hyperfine structure of $(3d)^5$ ions in crystal fields,” *Phys. Lett. A* **24**, 40 – 42 (1967).
- [58] M. Herlitschke, A. L. Tchougreff, A. V. Soudackov, B. Klobes, L. Stork, R. Dronskowski, and R. P. Hermann, “Magnetism and lattice dynamics of FeNCN compared to FeO ,” *New J. Chem.* **38**, 4670–4677 (2014).
- [59] N. A. Bogdanov, V. M. Katukuri, J. Romhányi, V. Yushankhai, V. Kataev, B. Büchner, J. van den Brink, and L. Hozoi, “Orbital reconstruction in nonpolar tetravalent transition-metal oxide layers,” *Nat. Comm.* **6**, 73061–73069 (2015).
- [60] K. Ishida, Y. Kitaoka, K. Asayama, S. Ikeda, S. Nishizaki, Y. Maeno, K. Yoshida, and T. Fujita, “Anisotropic pairing in superconducting Sr_2RuO_4 : Ru NMR and NQR studies,” *Phys. Rev. B* **56**, R505–R508 (1997).
- [61] J. Nichols, X. Gao, S. Lee, T. L. Meyer, J. W. Freeland, V. Lauter, D. Yi, J. Liu, D. Haskel, and J. R. Petrie, “Emerging magnetism and anomalous Hall effect in iridate-manganite heterostructures,” *Nat. Comm.* **7**, 12721 (2016).
- [62] J. Keil and H. Ehrlichmann, “Bunch Purity Measurements at PETRA III,” (7th International Particle Accelerator Conference, Busan (Korea), 8 May–13 May, 2016) pp. 3434–3436.
- [63] J. Klute, K. Balewski, A. Delfs, H. T. Duhme, M. Ebert, Ru. Neumann, and F. Obier, “The PETRA III Multi-bunch Feedback System,” (10th European Workshop on Beam Diagnostics and Instrumentation for Particle Accelerators, Hamburg (Germany), 16 May–18 May, 2011) pp. 494–496.
- [64] R.J. Nawrocky, U. Bergmann, and D.P. Siddons, “A bunch killer for the nsls x-ray electron storage ring,” in *Proceedings of International Conference on Particle Accelerators*, Vol. 3 (1993) pp. 2145–2147.
- [65] N.H. Sung, H. Gretarsson, D. Proepper, J. Porras, M. Le Tacon, A. V. Boris, B. Keimer, and B. J. Kim, “Crystal growth and intrinsic magnetic behaviour of Sr_2IrO_4 ,” *Philos. Mag.* **96**, 413–426 (2016).